PAPER

Check for updates

Microneedle patch with "spongy coating" to co-load multiple drugs to treat multidrug-resistant melanoma

Xinfang Li,† Weijiang Yu,† Jingshuang Yang, Yonghang Chen, Xuedan Qian, Jing Wang, Youxiang Wang [ID] * and Jian Ji [ID] *

Melanoma is the most aggressive skin malignancy that continues to increase in worldwide. The transferability and multidrug resistance lead to a high fatality rate. Synergistic administration of hydrophilic carboplatin (CBP) and hydrophobic vorinostat (SAHA) can be a reliable way to treat multidrug-resistant melanoma. However, the different physicochemical properties of multiple drugs make it difficult to achieve a convenient co-loading and an ideal synergistic treatment efficacy. To solve the problem, a microneedle patch with a porous "spongy coating" (PF-MNP) was fabricated. Firstly, (polyacrylic acid/polyethyleneimine)$_{10}$ multilayers were fabricated on polymethyl methacrylate MNP. Then a "spongy coating" was achieved by acid treatment and freeze-drying. Due to the capillary effect, hydrophobic SAHA and hydrophilic CBP could be conveniently adsorbed step-by-step. The two drugs could distribute evenly on the surface, and the morphology of MNP remained good. The loading content of SAHA and CBP was easily regulated by adjusting the concentration of the adsorption solution, and MNP could quickly release most drugs within 30 min. The final *in vivo* experiments proved that CBP/SAHA co-loaded PF-MNP had the best therapeutic efficiency for multidrug-resistant melanoma. The MNP with a "spongy coating" showed potential to be a safe and efficient transdermal delivery platform for multiple drugs.

1. Introduction

Melanoma is a potentially fatal skin malignancy and is one of the most aggressive diseases worldwide.[1–3] Nowadays, many developed treatments are used to fight against melanoma, such as surgery,[4] chemotherapy,[5–7] and radiation therapy.[8] Among them, chemotherapy has proven to be effective.[9,10] For example, carboplatin (CBP), a second generation platinum-based drug, has been widely used in clinics due to the broad anticancer spectrum and fewer side effects.[11,12] It can bind to the bases in the DNA double helix structure, allowing DNA molecules to produce intra- and inter-chain crosslinking. Then, the chemical structure of DNA is altered and thus affects the cell function.[12,13] However, systemic administration of the chemotherapy drug leads to a limited drug enrichment in the targeted tumor sites. Microneedle patch (MNP) is a transdermal drug delivery technology that newly appeared in recent years.[14] MNP can pierce the stratum corneum directly to promote transdermal drug delivery efficacy without pain,[15–17] making it an ideal platform to treat cutaneous illnesses. So MNP combined with chemotherapy can achieve an effective and targeted treatment against melanoma.[18]

On the other hand, multidrug resistance (MDR) is the most rigorous problem in chemotherapy.[19,20] Studies have shown that the combination of multiple chemotherapy drugs has a better therapeutic effect.[21,22] Vorinostat (SAHA), as an FDA-approved histone deacetylase inhibitor,[23,24] was used to solve the drug resistance of platinum drugs by weakening the interaction between histones and DNA.[25,26] Therefore, the combination of CBP and SAHA may represent a hopeful regimen for multidrug-resistant melanoma.[27,28] However, considering the different physicochemical properties of the two drugs, how to deliver hydrophobic SAHA and hydrophilic CBP at tumor sites simultaneously is a topic worth considering.

Layer-by-layer assembly technology, a simple and versatile technique, has been widely applied to fabricate functional coating in the biomedical field. Our previous research indicated that a multilayer film composed of polyethyleneimine (PEI) and polyacrylic acid (PAA) could form a porous spongy structure after acid treatment.[29] Due to the capillary effect, the porous film could adsorb both hydrophobic and hydrophilic drugs. So, in this research, MNP with a porous spongy coating

MOE Key Laboratory of Macromolecular Synthesis and Functionalization, International Research Center for X Polymers, Department of Polymer Science and Engineering, Zhejiang University, Hangzhou, 310027, P. R. China. E-mail: yx_wang@zju.edu.cn, jijian@zju.edu.cn
†These authors contributed equally to this work.

Scheme 1 The preparation process of ML-MNP and PF-MNP (A) and the adsorption process of SAHA and CBP (B).

was fabricated to co-load CBP and SAHA to treat the multi-drug-resistant melanoma. As shown in Scheme 1, polymethyl methacrylate (PMMA) MNP was firstly fabricated by a high-temperature method. Then $(PAA/PEI)_{10}$ multilayers were prepared by layer-by-layer self-assembly on a PMMA microneedle surface (ML-MNP). Then ML-MNP was immersed into acid solution with a pH value of 2.5 to form a porous structure (PF-MNP). The drug loading capacity and release profile of PF-MNP were tested. And the treatment efficiency of CBP/SAHA co-loaded PF-MNP was also verified on a multidrug-resistant melanoma model.

2. Experimental section

2.1. Chemicals

Polymethyl methacrylate (PMMA, M_n ~80 000), branched poly-ethyleneimine (PEI, MW ~25 000), polyacrylic acid (PAA, M_w ~100 000), Rhodamine 6G (Rh 6G) and fluorescein isothiocyanate isomer (FITC) were purchased from Aldrich Reagent Co., Ltd (Shanghai, China). Carboplatin (CBP), vorinostat (SAHA) and 7-hydroxycoumarin (7H Co) were purchased from FEIYUBIO Co., Ltd. The optimum cutting temperature (OCT) compound was purchased from Sakura Finetek Japan Co. Ltd (Hamacho, Japan). Polydimethylsiloxane (PDMS) molds of the microneedle patch (of about 1000 μm in height, 400 μm in width at base, 1000 μm of needle pitch, 10 × 10 array) were purchased from Taizhou Institute, Zhejiang University (China). Ultra-pure deionized water (Millipore, Direct Q® 3 UV) was used for all the tests. All of the chemicals were of analytical grade.

2.2. Synthesis of FITC-modified PEI

FITC-modified PEI (PEI-FITC) was synthesized as mentioned in previous research.[30] 2 ml of dimethyl sulfoxide (DMSO) that contained 31 mg of FITC was added drop by drop into 6 ml of DMSO that contained 1 g of PEI. The mixture was stirred for

24 h and then dialyzed for 3 d to remove the unreacted FITC. The PEI-FITC was finally obtained by freeze-drying. The graft ratio of FITC-PEI was calculated by the standard curve method.

2.3. Fabrication and characterization of a polyelectrolyte porous film on the surface of PMMA slice

A PMMA slice was fabricated with a high-temperature melting method in a vacuum environment as mentioned before.[31,32] Briefly, PMMA particles were arranged into the PDMS mold and melted in a vacuum environment at 230 °C for 6 h. After cooling to room temperature, the PMMA slice was demolded.

Firstly, the PMMA slice was pre-treated with a vacuum plasma deposition system for 240 s to promote surface hydrophilicity,[33,34] during which the air intake flow rate was about 40 mL min⁻¹. A contact angle measurement (DSA 100, Krüss, Germany) was used to test the hydrophilicity improvement of the PMMA surface.

$(PAA/PEI)_{10}$ multilayers were then fabricated on the PMMA slice by layer-by-layer self-assembly technology. In detail, the PMMA slice was alternately immersed into PEI solution (1 mg mL⁻¹, 15 min) and PAA solution (3 mg mL⁻¹, 15 min), separated by a 2 min purification in ultra-pure deionized water. After 10 cycles, the $(PAA/PEI)_{10}$ multilayers were treated with hydrochloric solution (pH = 2.5) for 30 min to induce the development of a microporous structure, then freeze-drying was applied to remove water. The PMMA slice with a porous film was marked as PF-slice in the research, and the PMMA slice with a multilayered coating was also fabricated as the control and marked as the ML-slice.

Surface topography from the top view and front view of the PF-slice and ML-slice was observed by a field emission scanning electron microscope (FE-SEM, HITACHI, S-4800). Meanwhile, the PF-slice after the adsorption of ethanol and ultra-pure deionized water was also photographed to observe the morphology change of the porous film.

2.4. Morphology of porous film coated microneedle patch

The microneedle patch with a porous spongy coating (PF-MNP) and the microneedle patch with multilayers (ML-MNP) were fabricated as for the PMMA slice. The morphology of PF-MNP and ML-MNP was observed by FE-SEM, and PF-MNPs that adsorbed ethanol and ultra-pure deionized water were also photographed.

2.5. Distribution of porous spongy coating and absorbed drugs

FITC-PEI was used to fabricate the ML-MNP and PF-MNP as mentioned before. Both ML-MNP and PF-MNP first adsorbed 8 mg mL^{-1} 7-hydroxycoumarin (7H Co) as a model hydrophobic drug, and then adsorbed 5 mg mL^{-1} rhodamine 6G (Rh 6G) as a model hydrophilic drug. These were marked as Rh 6G/7H Co@ML-MNP and Rh 6G/7H Co@PF-MNP, respectively. Then, Rh 6G/7H Co@ML-MNP and Rh 6G/7H Co@PF-MNP were photographed by a fluorescent microscope (BX61, Olympus, Japan) to observe the distribution of the porous coating and absorbed drugs on the surface of the MNP.

2.6. Drug loading capacity and release profile of single drug loaded PF-MNP

2.6.1. SAHA loading capacity and release profile. PF-MNPs first adsorbed SAHA in ethanol with different concentrations, 1 mg mL^{-1}, 4 mg mL^{-1} and 8 mg mL^{-1}, respectively. Then the SAHA loaded PF-MNPs (SAHA@PF-MNP) were treated with water to achieve the self-healing process of the porous coating. Then SAHA@PF-MNPs were immersed into 2 mL of phosphate buffered saline (PBS, pH = 7.4) and oscillated for 24 h. The concentration of the released SAHA was tested by a UV-Visible Spectrophotometer (UV-2600, SHIMADZU) and the total loading content was calculated by a standard curve method.

To test the release profile, SAHA@PF-MNPs with different loading contents were also immersed into PBS for 3 h. At 5, 10, 15, 30, 60, 120, and 180 min, 1 mL of the released solution was taken out and the concentration was also measured by a UV-Visible spectrophotometer and calculated by the standard curve method. At the same time, 1 mL of fresh PBS was added. For each test, all the samples were prepared in triplicate.

2.6.2. CBP loading capacity and release profile. PF-MNPs were first treated with ethanol and then adsorbed carboplatin in water with different concentrations at 1 mg mL^{-1}, 5 mg mL^{-1} and 10 mg mL^{-1}. Then the loading content and drug release profile of CBP loaded PF-MNPs (CBP@PF-MNP) were tested as mentioned above. For each test, all the samples were prepared in triplicate.

2.7. Drug loading and release profile of SAHA/CBP@PF-MNP

PF-MNPs adsorbed SAHA in ethanol with a concentration of 8 mg mL^{-1} firstly and then adsorbed CBP in water with a concentration of 5 mg mL^{-1} to achieve a co-loading of the two drugs. Then CBP/SAHA@PF-MNPs were immersed into PBS for 1 h, 1 mL of the released solution was taken out at 5 min, 15 min, 30 min and 60 min and tested by an Inductive Coupled Plasma Emission Spectrometer (ICP, 730-ES, Varian, USA) to test the cumulative release of CBP.

2.8. In vitro skin insertion capacity

Rh 6G/7H Co@PF-MNP and Rh 6G/7H Co@ML-MNP were attached to a porcine cadaver skin to test the insertion ability by a frozen section test. After being inserted by MNPs for 30 min, the skin was cleaned and frozen at −80 °C, then embedded in an optimal cutting temperature compound (OCT). After that, frozen samples were cut into 10 μm slices by a freezing microtome (CryoStar NX50, Thermo, USA) and photographed with a fluorescent microscope (BX61, Olympus, Japan) to test the delivery of 7H Co, Rh 6G and PEI-FITC in the skin within 30 min. The holes created by the MNP could be observed and the average depth was measured by ImageJ.

2.9. In vivo anti-tumor experiment

The anti-tumor efficacy was tested with an in vivo experiment on tumor-bearing mice. To set up the tumor model, human CBP-resistant melanoma cells (A375-DDP) dispersed in PBS (pH = 7.4; 100 μL, 5 × 10^6 cells) were injected into the right flank of BALB/c nude mice subcutaneously. After the tumor volume reached around 100 mm^3, tumor-bearing mice were randomly divided into five groups (n = 5 per group): (1) untreated group, in which the tumor-bearing mice were untreated; (2) CBP/SAHA@PF-MNP treated group, in which the tumor-bearing mice were treated by one CBP/SAHA@PF-MNP dose each time; (3) CBP@PF-MNP treated group, in which the tumor-bearing mice were treated by one CBP@PF-MNP dose each time; (4) SAHA@PF-MNP treated group, in which the tumor-bearing mice were treated by one SAHA@PF-MNP dose each time; (5) CBP/SAHA IN group, in which the tumor-bearing mice were intravenously injected with 100 μL of a CBP/SAHA mixture. According to the total loading content of SAHA/CBP@PF-MNP, the administration dosage of the intravenous injection group was 475.4 μg of CBP and 250.6 μg of SAHA each time.

All the treatments were conducted once a week and repeated for 3 weeks (day 0, day 7, and day 14). The tumor volume and body weight of the mice were tracked for 21 d. The tumor volume was calculated by the formula: tumor volume = $0.5 \times length \times width^2$. After 21 d of treatment, tumor-bearing mice were sacrificed to obtain the isolated tumors and isolated tumors of each group were weighed. The tumor inhibition efficacy for each group was calculated by the formula: tumor inhibition efficacy = $(1 - W_1/W_2) \times 100\%$. W_1 refers to the excised tumor weight of the treated groups and W_2 refers to the excised tumor weight of the untreated group.[35] Then the isolated tumors from different groups were fixed in 4% formaldehyde for histological analysis. And H&E, Ki67, and TUNEL assays were further employed to detect the subsequent proliferation and apoptosis state.

The used microneedle patches were also recycled and then immersed into PBS for 24 h. The concentration of CBP in the released solution was tested by a UV-visible spectrophoto-

meter, and the actual CBP administration dosage could be calculated by a subtraction method.

All the animal experiments were carried out according to the "Principles of Laboratory Animal Care" (NIH publication no. 86-23, revised 1985) and the guidelines for Animal Care and Use Committee, Zhejiang University. Healthy male BALB/c nude mice (4–5 weeks old, weight around 15 g) were supplied by the animal center of Zhejiang Academy of Medical Sciences and the Shanghai SLAC Laboratory Animal Co. Ltd.

2.10. Statistical analysis

For this study, all the values are presented as their mean ± standard deviation. Statistical differences are considered to be significant when $p < 0.05$.

3. Results and discussion

3.1. Topography of the flat porous film

A flat porous coating was fabricated on the PMMA slice first. Due to the hydrophobicity, the PMMA surface was treated by a vacuum plasma deposition system. The water contact angle decreased from 82° to 9.7°, which proved that the hydrophilicity of the PMMA surface improved significantly.

The topography of the PF-slice and ML-slice could also be observed by SEM. As shown in Fig. 1, the surface of the ML-slice was smooth before acid treatment. After being exposed to an acid solution with a pH value of 2.5 for 30 min, a rough and porous structure appeared, and the thickness of the multilayers increased from 6 μm to 30 μm. According to the thickness, the porosity was calculated to be around 80%. Some research had explored the reason for the induced appearance of the porous structure.[36–38] Our previous research hypothesized that this phenomenon was attributed to the protonation of PAA.[29] The COOH/COO⁻ ratio increased in a low pH environment. Then part of ion pairs between PAA and PEI dissociated, and the mobilization of the polyelectrolyte chains induced the formation of a porous structure. The porous structure remained after ethanol absorption, whereas a self-healing process was achieved after water adsorption. This phenomenon was attributed to the high permittivity of water. It had a shielding effect of the charges on the macromolecular chains and increased the free volume between the molecular chains. So, macromolecular chains were reorganized, and the porous structure disappeared. On the contrary, the porous structure would remain when exposed to organic solvents with a low permittivity.

3.2. Morphology of MNPs

The morphology of PF-MNP and ML-MNP was observed by SEM. As shown in Fig. 2, the films on the MNP had the same appearance as that on the flat. The microneedles kept their good cylindrical shape during the entire coating preparation and drug loading process.

3.3. Distribution of coating film and simulate drugs

PEI-FITC was utilized to mark the coating films on ML-MNP and PF-MNP, and Rh 6G and 7H Co were selected as the model drugs to be adsorbed on the PF-MNP. The grafting ratio of FITC-PEI was calculated to be 45%. Due to the capillary effect, the porous spongy coating adsorbed both the hydrophobic 7H Co and hydrophilic Rh 6G quickly. From the fluorescent images in Fig. 3B, model drugs could distribute uniformly on the surface of PF-MNP. Even on the top of microneedles, the fluorescence of the model drugs could also be observed. The multilayers were stable during the coating preparation and drug loading process. Compared with the PF-MNP, the ML-MNP could not adsorb drugs since there was no porous structure. So, no fluorescence of the model drugs is observed in Fig. 3D.

Fig. 1 SEM images of top view (A) and front view (B) topography of the ML-slice and PF-slice after adsorbing ethanol and water.
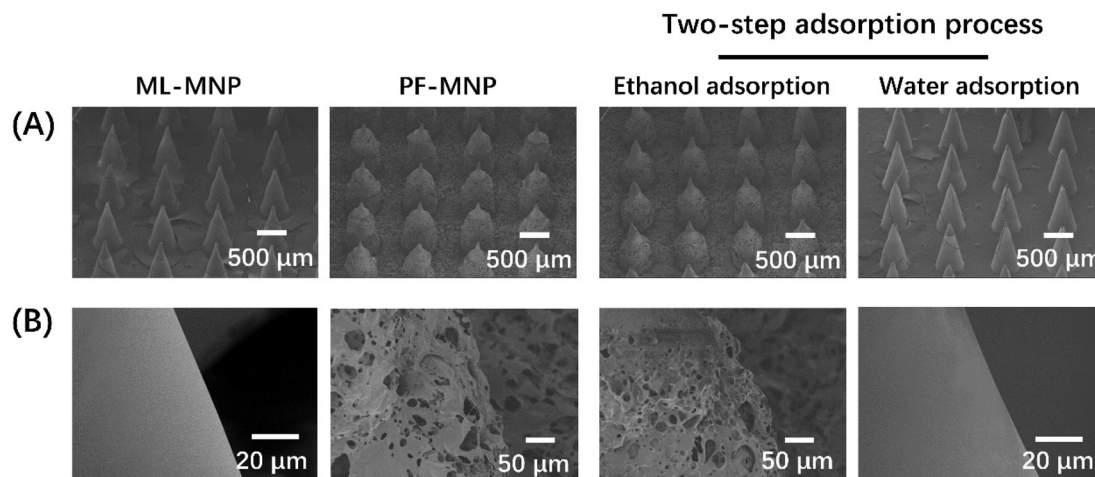
Two-step adsorption process

Fig. 2 SEM images of the overall (A) and partial (B) morphology of ML-MNP, PF-MNP, and PF-MNP after adsorbing ethanol and water.
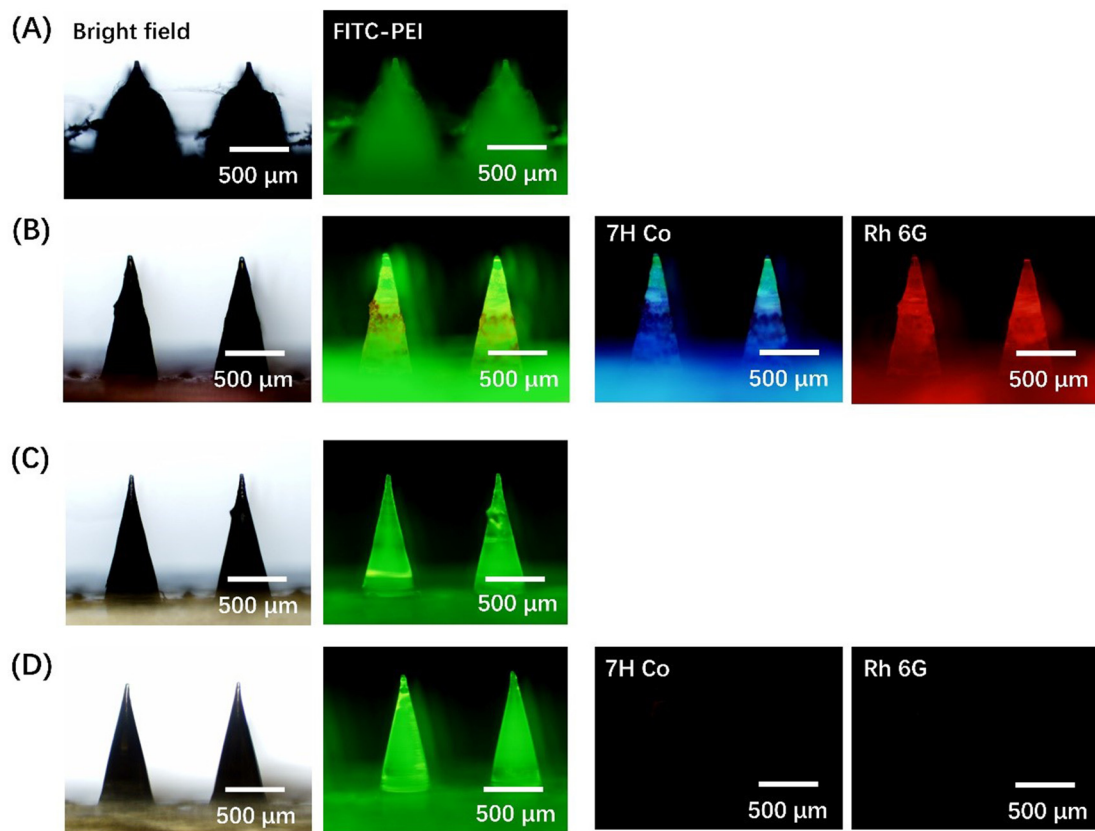

Fig. 3 Fluorescent images of PF-MNP (A), Rh 6G/7H Co@PF-MNP (B), ML-MNP (C) and Rh 6G/7H Co@ML-MNP (D) (green: PEI-FITC; blue: 7H Co; red: Rh 6G).

3.4. Drug loading capacity and release profile of PF-MNPs

3.4.1. Individual drug loading capacity and release profile of SAHA and CBP. SAHA in ethanol and CBP in water with different concentrations were separately adsorbed by PF-MNP as mentioned before. As shown in Fig. 4A, the total CBP loading contents of CBP@PF-MNP at concentrations of 1 mg mL^{-1}, 5 mg mL^{-1} and 10 mg mL^{-1} were about 332.7 μg per array, 475.4 μg per array, and 735.2 μg per array, respectively. Additionally, the total SAHA loading content of SAHA@PF-MNP at concentrations of 1 mg mL^{-1}, 4 mg mL^{-1} and 8 mg mL^{-1} were about 88.5 μg per array, 145 μg per array
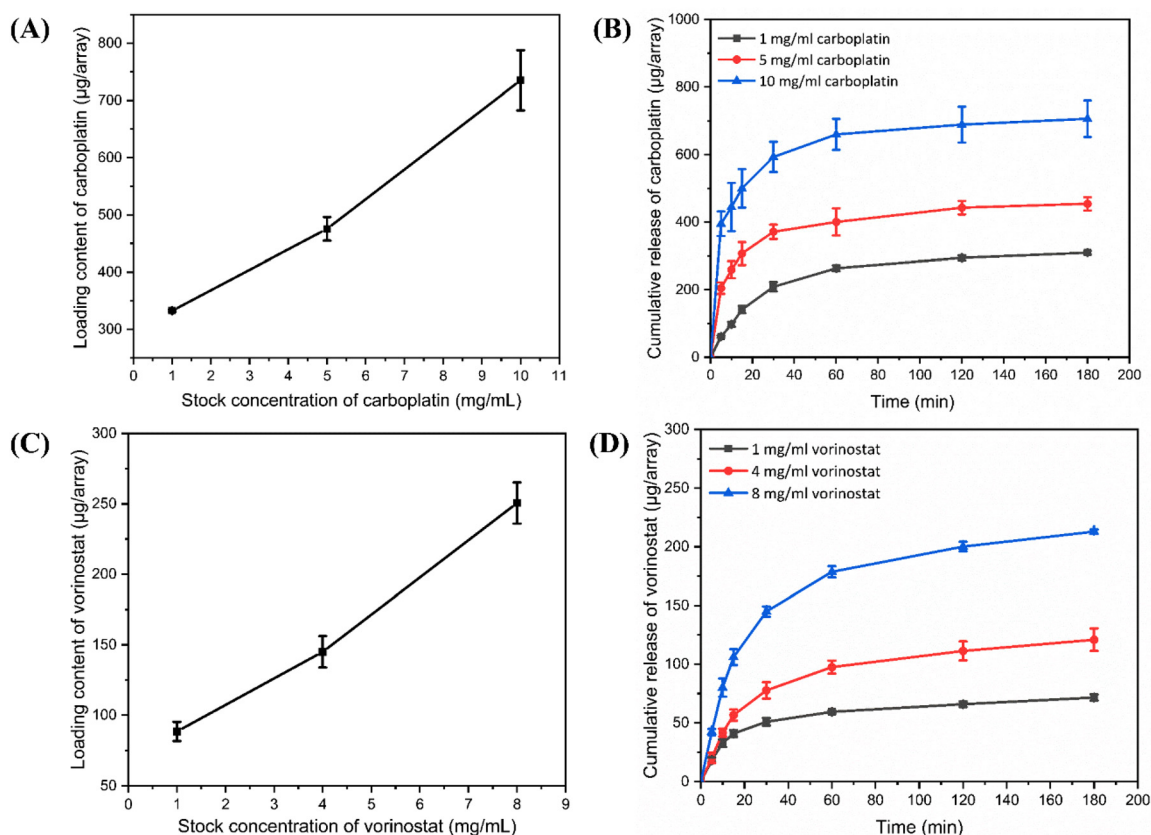
Fig. 4 The total drug loading content of CBP@PF-MNP (A) and SAHA@PF-MNP (C) with different concentrations of the adsorbed solution. The drug release profile within 3 h of CBP@PF-MNP (B) and SAHA@PF-MNP (D) with different concentrations of the adsorption solution.

and 250.6 μg per array (Fig. 4C), respectively. The total loading content of CBP and SAHA on PF-MNP increased linearly with the ascent of drug concentration in the absorption solution. This result showed that the loading content of the hydrophilic and hydrophobic drugs could be easily controlled by adjusting the concentration of the drug absorption solution.

From Fig. 4B and D, the PF-MNP had a quick drug release within the initial 30 min and slowed down as time increased. CBP@PF-MNP could release about 73% CBP, and the SAHA@PF-MNP could release about 55% SAHA of the total loading content within 30 min. To meet the required administration dosage, the concentration of the CBP adsorption solution was chosen as 5 mg mL^{-1} and SAHA in ethanol was chosen as 8 mg mL^{-1} in the following experiments. In addition, the total drug loading content of CBP and SAHA were 475.4 μg per array and 250.6 μg per array, respectively.

3.4.2. CBP release profile from CBP/SAHA@PF-MNP. CBP/SAHA@PF-MNPs were used to test whether the first loading of SAHA would affect the subsequent load of CBP. As shown in Fig. 5, the release profile of CBP from CBP/SAHA@PF-MNP was consistent with that from CBP@PF-MNP within 1 h. So, the loading process of SAHA and CBP would not affect each other and the loading capacity of SAHA and CBP that were tested separately (see above) was reliable. On the basis of the drug release profile and patient compliance, the adminis-
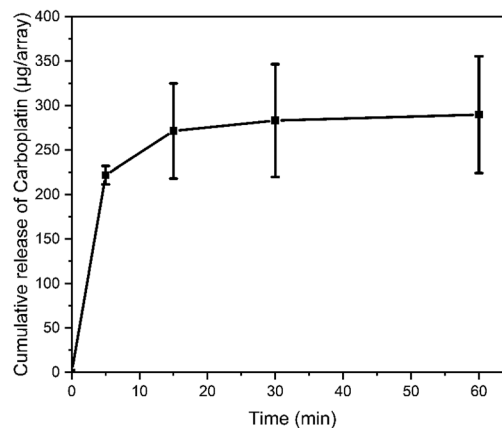

Fig. 5 The CBP release profile of CBP/SAHA@PF-MNP within 1 h as tested by an Inductive Coupled Plasma Emission Spectrometer (ICP).

tration time in the following experiments was chosen as 30 min, during which the released amount of drugs achieved the required dosage.

3.5. Skin insertion capacity

Rh 6G/7H Co@PF-MNP and Rh 6G/7H Co@ML-MNP were inserted into the porcine cadaver skin for 30 min. The cross

section of the isolated skin was stained by hematoxylin–eosin to test the insertion capability of the microneedles. As shown in Fig. 6A, Rh 6G/7H Co@PF-MNP successfully pierced the stratum corneum, and the insertion depth was about 325 μm.
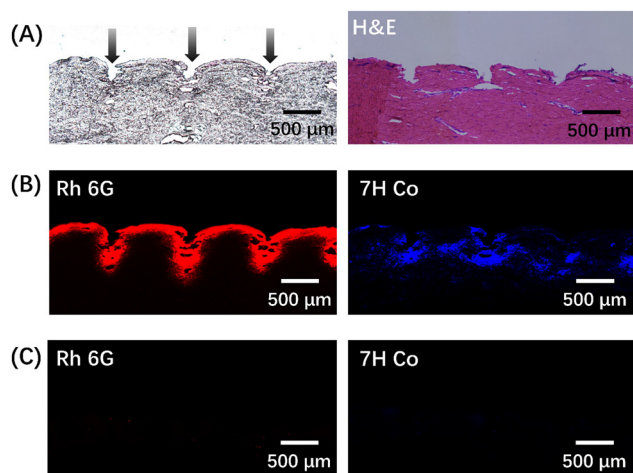

Fig. 6 (A) Bright field images of the cross section of isolated skin inserted with Rh 6G/7H Co@PF-MNP before and after H&E staining. Fluorescent images of the cross section of isolated skin inserted with Rh 6G/7H Co@PF-MNP (B) and Rh 6G/7H Co@ML-MNP (C) (blue: 7H Co; red: Rh 6G).

Cross sections were photographed by a fluorescent microscope and the distribution of the model drugs under skin could be observed. From Fig. 6B, it can be visually illustrated that Rh 6G and 7H Co released quickly from PF-MNP and were delivered into skin within 30 min. In comparison, with Rh 6G/7H Co@ML-MNP (Fig. 6C), no fluorescence could be observed in the skin. Due to the lack of porous structure in surface of ML-MNP, Rh 6G and 7H Co could not actually load on ML-MNP. The result confirmed that the microneedle patch with a porous spongy coating had the potential to be a drug loading platform to realize a quick transdermal delivery.

### 3.6. *In vivo* anti-tumor evaluation of multidrug-resistant melanoma

A subcutaneous tumor model was established on BALB/c nude mice. When the tumor volume grew to approximately 100 mm³, tumor-bearing mice were randomly divided into five groups ($n = 5$) as mentioned before. The tumor volume and body weight were recorded for 21 d, and isolated tumors were dissected out to calculate the antitumor efficacy after treatment. The mice in the untreated group were sacrificed at 18 d as otherwise the tumor volume would so big as to violate the ethics of animal experiments.

As shown in Fig. 7A, subcutaneous tumors of mice in the SAHA/CBP intravenous injection group (CBP: 31.7 mg kg⁻¹;
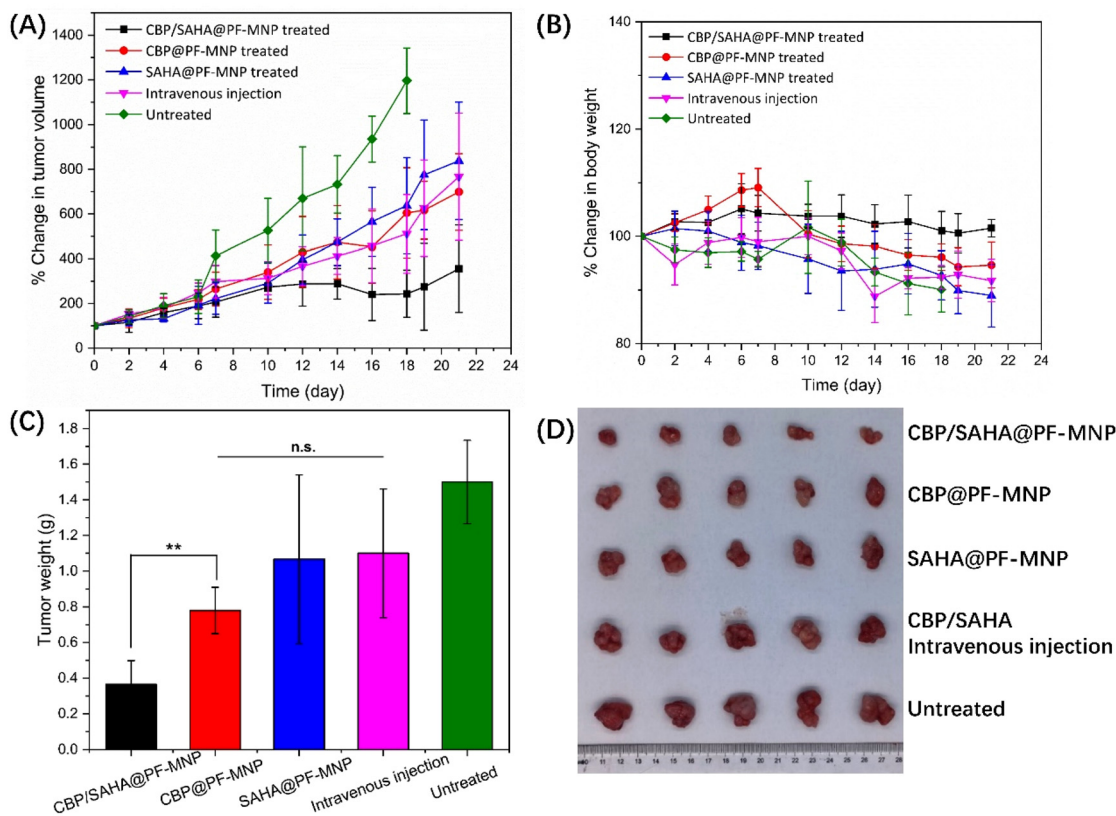
Fig. 7 (A) Change of tumor volume of five groups within 21 d of treatment; (B) change of mice body weight in the five groups within 21 d of treatment; (C) weight of tumor that isolated from mice in a different set of five groups after 21 d of treatment; (D) image of the isolated tumors of five groups after 21 d of treatment.
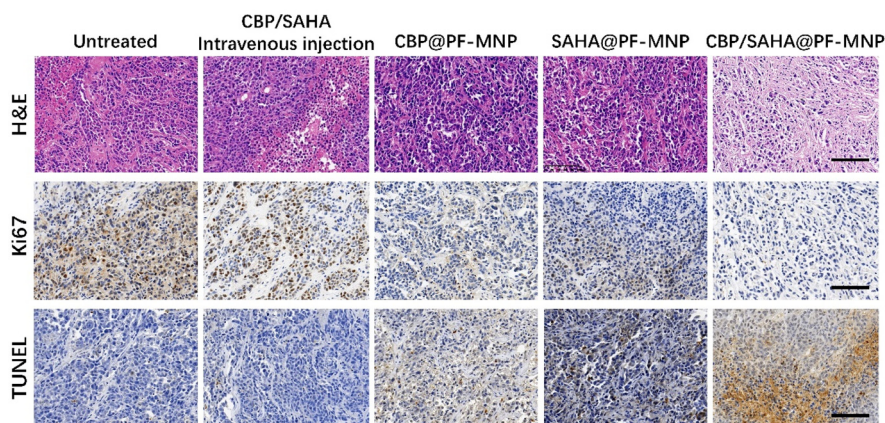
Fig. 8 Representative images of H&E, Ki67, and TUNEL stained tumor tissues isolated from the tumor-bearing mice after treatment by CBP/SAHA intravenous injection, CBP@PF-MNP, SAHA@PF-MNP and CBP/SAHA@PF-MNP. The untreated group was conducted as the control. The Ki67-positive proliferating cells and TUNEL-positive apoptotic cells are stained brown. Scale bar: 100 μm.

SAHA: 16.7 mg kg^{-1}), SAHA@PF-MNP (SAHA: 16.7 mg kg^{-1}) treated group and CBP@PF-MNP treated group (CBP: 31.7 mg kg^{-1}) were only inhibited slightly. For the SAHA/CBP intravenous injection group, the tumor volume was 766% of the initial state and antitumor efficacy was calculated to be only 26.7%. Since systemic administration of chemotherapy led to a limited drug enrichment in the targeted melanoma, the SAHA/CBP intravenous injection had the worst therapeutic effect. As mentioned before, the administration of CBP or SAHA alone had limited efficacy to treat drug-resistant tumor. The tumor volumes of the SAHA@PF-MNP group and the CBP@PF-MNP group were about 838% and 698% of the initial state, respectively. And the antitumor efficacy was calculated to be 28.9% and 48%, respectively, although mice in these two groups were treated *in situ*. However, the synergistic administration of CBP/SAHA@PF-MNP (CBP: 31.7 mg kg^{-1}; SAHA: 16.7 mg kg^{-1}) could effectively overcome the multidrug resistance and improve antitumor efficacy. Tumor volume was only 355% of the initial state and the antitumor efficacy could reach 75.6% after treatment. The image of isolated tumors in Fig. 7D is consistent with the therapeutic effect of different groups. The used CBP/SAHA@PF-MNPs were recycled to test the remaining content of CBP. Additionally, the actual administration dosage of CBP was calculated to be 236 μg per array by a subtraction method.

Fig. 7B shows the body weight of mice in different groups. Except for the CBP/SAHA@PF-MNP treated group, the weight of the mice in the other three groups had a downward trend, which illustrates that the health of the mice was undermined.

To further explore the antitumor efficiency of CBP/SAHA@PF-MNP, H&E, Ki67 and TUNEL immunohistochemistry were used to analyze the degree of tumor proliferation and apoptosis in different groups. As shown in Fig. 8, it can be observed that the CBP/SAHA@PF-MNP treated group had the worst tumor cell proliferation effect, so it showed the best therapeutic efficiency. The result is consistent with the antitumor efficiency calculated by the isolated tumor weight.

4. Conclusions

In this research, PMMA MNP was first fabricated by a high-temperature melting method in a vacuum environment. The $(PAA/PEI)_{10}$ multilayer was coated on a microneedle surface by a layer-by-layer self-assembly technology. Then, multilayers were treated in an acid environment to induce a porous spongy structure, which could absorb multiple drugs by a capillary effect. The porous structure remained in an organic solvent and could achieve a self-healing process in water. So, the PF-MNP could load hydrophobic SAHA in ethanol and hydrophilic CBP in water step by step. And the total loading content was easily controlled by adjusting the concentration of the drug absorption solution. According to the required administration dosage, the concentration of drug solution was chosen as 5 mg mL^{-1} CBP in water and 8 mg mL^{-1} SAHA in ethanol. The total loading content of SAHA/CBP@PF-MNP was around 250.6 μg per array SAHA and 475.4 μg per array CBP, and around 55% SAHA and 73% CBP would be released within 30 min. In the following *in vivo* antitumor experiments with drug-resistant melanoma, SAHA/CBP@PF-MNP showed the best therapeutic effect, and the antitumor efficacy was calculated to be 75.6%.

In conclusion, MNP with a porous spongy coating could be successfully fabricated and achieve the synergistic administration of SAHA and CBP to a multidrug-resistant melanoma. It settled the difficulty of co-loading hydrophilic and hydrophobic drugs on a microneedle patch, and showed potential to be a safe and efficient on-demand transdermal drug delivery platform for many kinds of drugs and biomacromolecules.

Author contributions

Xinfang Li: Conceptualization, methodology, validation, formal analysis, investigation, data curation, writing – original draft, visualization. Weijiang Yu: Methodology, validation,

investigation, writing – original draft. Jingshuang Yang: Validation, formal analysis, investigation. Yonghang Chen: Investigation, data curation. Xuedan Qian: Investigation, data curation. Jing Wang: Methodology, validation. Youxiang Wang: Supervision, writing – review & editing, funding acquisition. Jian Ji: Supervision, project administration, writing – review & editing, funding acquisition.

Conflicts of interest

There are no conflicts of interest to declare.

Acknowledgements

References

1 H. Pomerantz, D. Huang and M. A. Weinstock, *J. Am. Acad. Dermatol.*, 2015, **72**, 794–800.

2 R. F. Wagner and L. Nathanson, *J. Am. Acad. Dermatol.*, 1986, **14**, 249–256.

3 S. Carr, C. Smith and J. Wernberg, *Surg. Clin. North Am.*, 2020, **100**, 1–12.

4 T. A. Kaspar and R. F. Wagner, *Cutis*, 1992, **50**, 350–351.

5 R. J. Green and L. M. Schuchter, *Hematol. Oncol. Clin. North Am.*, 1998, **12**, 863–875.

6 A. Gupta, F. Gomes and P. Lorigan, *Melanoma Manage.*, 2017, **4**, 125–136.

7 G. Song, G. Jiang, T. Liu, X. Zhang, Z. Zeng, R. Wang, P. Li and Y. Yang, *ACS Biomater. Sci. Eng.*, 2020, **6**, 4116–4125.

8 A. R. Harwood and B. J. Cummings, *Cancer Treat. Rev.*, 1981, **8**, 271–282.

9 B. S. Kalal, D. Upadhya and V. R. Pai, *Oncol. Rev.*, 2017, **11**, 19–25.

10 J. M. Gasent Blesa, E. Grande Pulido, V. Alberola Candel and M. Provencio Pulla, *Am. J. Clin. Oncol.*, 2011, **34**, 179–187.

11 G. F. de Sousa, S. R. Wlodarczyk and G. Monteiro, *Braz. J. Pharm. Sci.*, 2014, **50**, 693–701.

12 L. Kelland, *Nat. Rev. Cancer*, 2007, **7**, 573–584.

13 D. Wang and S. J. Lippard, *Nat. Rev. Drug Discovery*, 2005, **4**, 307–320.

14 P. Carter, B. Narasimhan and Q. Wang, *Int. J. Pharm.*, 2019, **555**, 49–62.

15 M. Yamada and T. W. Prow, *Adv. Drug Delivery Rev.*, 2020, **153**, 2–17.

16 A. F. Moreira, C. F. Rodrigues, T. A. Jacinto, S. P. Miguel, E. C. Costa and I. J. Correia, *Pharmacol. Res.*, 2019, **148**, 104438.

17 C. Wang, Y. Ye, G. M. Hochu, H. Sadeghifar and Z. Gu, *Nano Lett.*, 2016, **16**, 2334–2340.

18 S. Indermun, R. Luttge, Y. E. Choonara, P. Kumar, L. C. du Toit, G. Modi and V. Pillay, *J. Controlled Release*, 2014, **185**, 130–138.

19 M. Kanamala, W. R. Wilson, M. Yang, B. D. Palmer and Z. Wu, *Biomaterials*, 2016, **85**, 152–167.

20 C. Holohan, S. Van Schaeybroeck, D. B. Longley and P. G. Johnston, *Nat. Rev. Cancer*, 2013, **13**, 714–726.

21 Q. Hu, W. Sun, C. Wang and Z. Gu, *Adv. Drug Delivery Rev.*, 2016, **98**, 19–34.

22 S. Xu, X. Zhu, W. Huang, Y. Zhou and D. Yan, *J. Controlled Release*, 2017, **266**, 36–46.

23 B. S. Mann, J. R. Johnson, M. H. Cohen, R. Justice and R. Pazdur, *Oncologist*, 2007, **12**, 1247–1252.

24 T. K. Owonikoko, S. S. Ramalingam, B. Kanterewicz, T. E. Balius, C. P. Belani and P. A. Hershberger, *Int. J. Cancer*, 2010, **126**, 743–755.

25 J. Shen, C. Huang, L. Jiang, F. Gao, Z. Wang, Y. Zhang, J. Bai, H. Zhou and Q. Chen, *Biochem. Pharmacol.*, 2007, **73**, 1901–1909.

26 M. S. Kim, M. Blake, J. H. Baek, G. Kohlhagen, Y. Pommier and F. Carrier, *Cancer Res.*, 2003, **63**, 7291–7300.

27 J. Martinez-Useros, M. Martin-Galan, M. Florez-Cespedes and J. Garcia-Foncillas, *Cancers*, 2021, **13**(13), 3209.

28 Y. Xiong, Y. Zhao, L. Miao, C. M. Lin and L. Huang, *J. Controlled Release*, 2016, **244**, 63–73.

29 X.-C. Chen, K.-F. Ren, W.-X. Lei, J.-H. Zhang, M. C. L. Martins, M. A. Barbosa and J. Ji, *ACS Appl. Mater. Interfaces*, 2016, **8**, 4309–4313.

30 J. Li, L. Zheng, H. Cai, W. Sun, M. Shen, G. Zhang and X. Shi, *Biomaterials*, 2013, **34**, 8382–8392.

31 X. Li, Q. Xu, J. Wang, P. Zhang, Y. Wang and J. Ji, *J. Mater. Chem. B*, 2021, **9**, 5528–5536.

32 J. H. Park, M. G. Allen and M. R. Prausnitz, *J. Controlled Release*, 2005, **104**, 51–66.

33 K. Nair, B. Whiteside, C. Grant, R. Patel, C. Tuinea-Bobe, K. Norris and A. Paradkar, *Pharmaceutics*, 2015, **7**, 471–485.

34 M. J. Uddin, N. Scoutaris, P. Klepetsanis, B. Chowdhry, M. R. Prausnitz and D. Douroumis, *Int. J. Pharm.*, 2015, **494**, 593–602.

35 Z. Li, H. Wang, Y. Chen, Y. Wang, H. Li, H. Han, T. Chen, Q. Jin and J. Ji, *Small*, 2016, **12**, 2731–2740.

36 J. D. Mendelsohn, C. J. Barrett, V. V. Chan, A. J. Pal, A. M. Mayes and M. F. Rubner, *Langmuir*, 2000, **16**, 5017–5023.

37 J. L. Lutkenhaus, K. McEnnis and P. T. Hammond, *Macromolecules*, 2008, **41**, 6047–6054.

38 X. Chen and J. Sun, *Chem. – Asian J.*, 2014, **9**, 2063–2067.